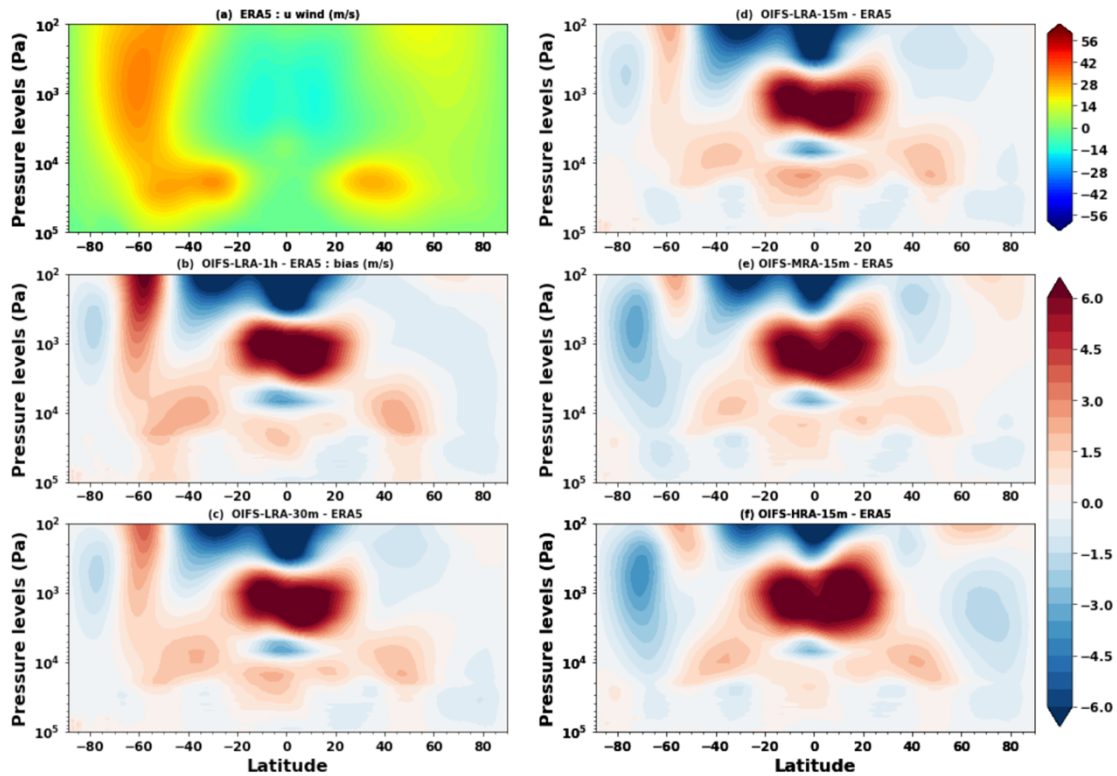


59 the lower stratosphere is larger in the high resolution (i.e., OIFS-HRA-15m), and the warm bias above the
 60 stratosphere is smaller compared to the other configurations. Robert et al. (2018) noticed a similar zonal mean
 61 temperature bias and speculated that the zonal mean temperature bias is linked with the sensitivity of spurious
 62 mixing due to convection and diffusion.”



64 **Figure 4.** (a) Annual zonal mean ERA5 zonal wind [ms^{-1}]. (b-d) Annual zonal mean zonal wind [ms^{-1}] bias for
 65 different model time steps (1h (b), 30m (c), and 15m (d)) using ~ 100 km resolution, and (e-f) with different
 66 horizontal resolutions, ~ 50 (e) and ~ 25 km (f), respectively. Biases are computed with respect to ERA5 over the
 67 period 1979–2019.

68
 69
 70 (2) The abstract concludes with the general statement that "reducing the time step in the OpenIFS model, one
 71 can alleviate some climate biases at a lower cost than by increasing the horizontal resolution." I would like the
 72 authors to add some discussion of whether they expect their results to generalise to resolutions and/or time-
 73 steps not tested in this manuscript. For example, how far is the LR configuration from converging? Would
 74 reducing time-step in a much higher resolution model (e.g. 9km) bring similar benefits? Depending on these
 75 additions, the authors may wish to qualify the concluding line of the abstract.

76 As suggested by the reviewer, we have modified the general conclusion to more specific as (lines 28-29):
 77 “Reducing the time step in the coarse resolution (~ 100 km) OpenIFS model, one can alleviate some climate
 78 biases at a lower cost than by increasing the horizontal resolution.”

79
 80 (3) What is the impact time-step/resolution on the representation of extremes? It is plausible that changes in
 81 time-step that improve the mean state have a limited impact on extremes that are more sensitive to horizontal
 82 resolution (e.g. orographic precipitation or tropical cyclones). As cited by the authors, the mean climate of the
 83 25km and 50 km HighResMIP configurations of IFS are very similar. However, the differences in horizontal
 84 resolution are evident in the representation of extremes (examples below):

85 <https://agupubs.onlinelibrary.wiley.com/doi/full/10.1029/2019JD032184>

86 Bador et al. (2020)

87 <https://journals.ametsoc.org/view/journals/clim/33/7/jcli-d-19-0639.1.xml>

88 Roberts J. et al (2020)

89 This is an excellent point. However, the main focus in this study is the mean state biases. The OpenIFS’ model
 90 time-step sensitivity to extremes will be discussed in detail in a separate manuscript.

91

92 **Minor comments:**

93 Introduction: This section would benefit from an overview of the "expected" impacts of reducing time-step in
94 simple models in terms of truncation error and how this might not always hold true in a more complex system.
95 For example, in simple finite difference models, solutions converge as grid-spacing and time-step are decreased
96 due to reduced truncation errors. The choice of time-step and grid-spacing may also be constrained by stability
97 criteria. However, this intuition does not always hold in complex models due to the coupling between many
98 different elements. For instance, it is plausible that the unconditionally stable semi-implicit semi-Lagrangian
99 scheme used in the IFS allows a user to configure the model with a long time step to reduce the cost. Later
100 developments on top of this configuration introduce compensating errors in other aspects of the physics that
101 reduce biases. Reducing the time step at a later stage may then leads to increased biases as the model
102 configuration has been implicitly tuned for a particular combination of time-step and resolution.

103 We added some text to the Introduction section (see below) (lines 75-82):

104 “While the semi-implicit semi-Lagrangian scheme, as used in OpenIFS, is unconditionally stable and the time
105 step can be chosen to be very long, a shorter time step generally leads to a decrease in truncation error in the
106 finite differences and thus a more accurate representation of the model dynamics. The physics
107 parameterisations, which are computed independently of each other in OpenIFS, also benefit from a shorter time
108 step as it will allow the various parameterisations to be coupled at a higher frequency (Beljaars et al. 2018).
109 However, model parameters for e.g., convection or diffusion may be tuned for a specific time step and
110 shortening the time step can therefore, in some cases, increase model error. Hence, a shorter model time step is
111 expected to reduce biases in model dynamics, e.g., winds, while the results for parameterised processes, e.g.,
112 precipitation, may be mixed”.

113
114 Lines 110-119. The authors state that their "detailed analysis of phase speed in such a manner is novel in
115 literature". This may be the case, but I would like the authors to provide a more detailed summary of the method
116 used to diagnose the amplitude and phase speed of extratropical Rossby waves (e.g. a bullet point list of the
117 main processing steps). The current description is insufficient for reproduction of the analysis. In particular, it is
118 not clear from the text how wave packets and associated phase speeds are diagnosed.

119 We revised the texts so that we can reproduce the analysis by following the steps (lines 132-137)

120 “We then applied the Fourier decomposition analysis to determine amplitude and position for each Rossby wave
121 number at each latitude as a function of time. Phase speed is computed as the difference in the daily position of
122 each wave, and stored at the midpoints in the time dimension. For consistency, wave amplitudes are interpolated
123 to the midpoints in time as well. Lastly, seasonal averages are computed from the daily data for the boreal and
124 austral winter seasons over the time period 1979–2019. In the case of phase speed, it is weighed by the
125 corresponding daily (midpoint) amplitude squared when computing the seasonal averages in order to account for
126 the impact of higher-amplitude events.”

127
128 Line 169. Typo? Should be "Roberts et al. (2018)" as in intro?

129 This has been fixed.

130

131 Line 198. Is it correct to include Coriolis? Work done by Coriolis term should be zero since it acts perpendicular
132 to motion of air parcels.

133

134 Yes, the Coriolis term is included in the DYN part because we are analyzing zonal wind tendency. However, we
135 have not quantified the individual contribution of the Coriolis term to the DYN term.

136

137 Lines 226-228: It is possible that the lower precipitation RMSE in OIFS-LRA-1h is due to a "double penalty"
138 effect that penalises higher resolution models, which have more structure in the precipitation fields. Is the
139 precipitation in the LR-1h experiment notably smoother? Other metrics (e.g. fractions skill score) may provide a
140 different ranking of models. More details on double-penalty effects and fraction skill score here:

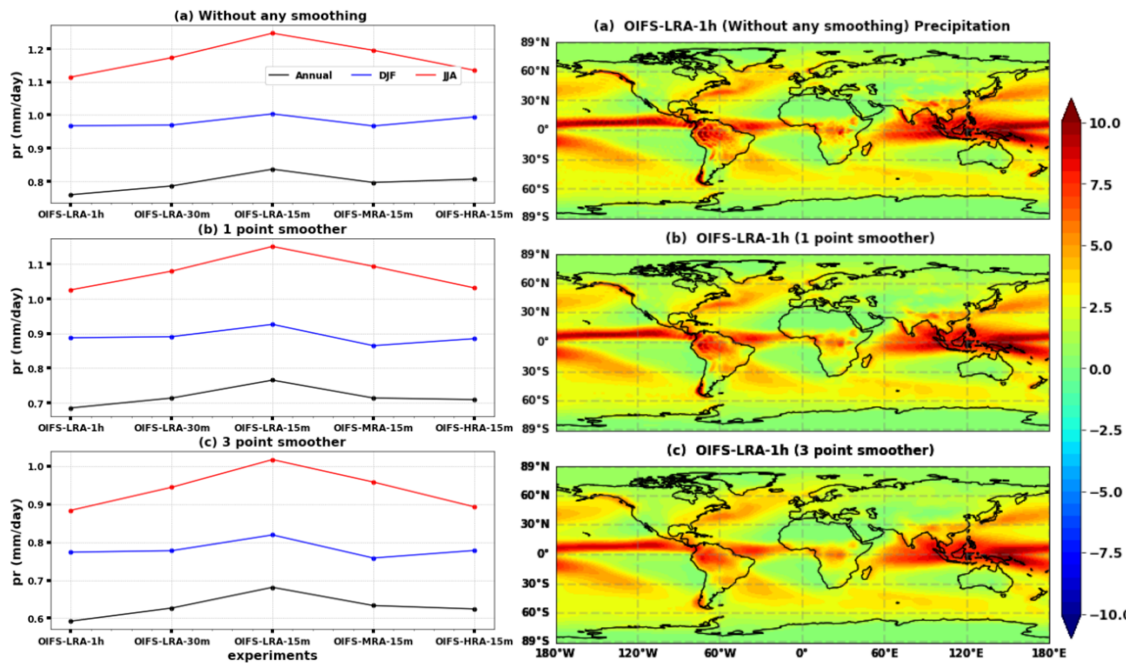
141 <https://www.ecmwf.int/en/about/media-centre/science-blog/2023/verifying-high-resolution-forecasts>

142

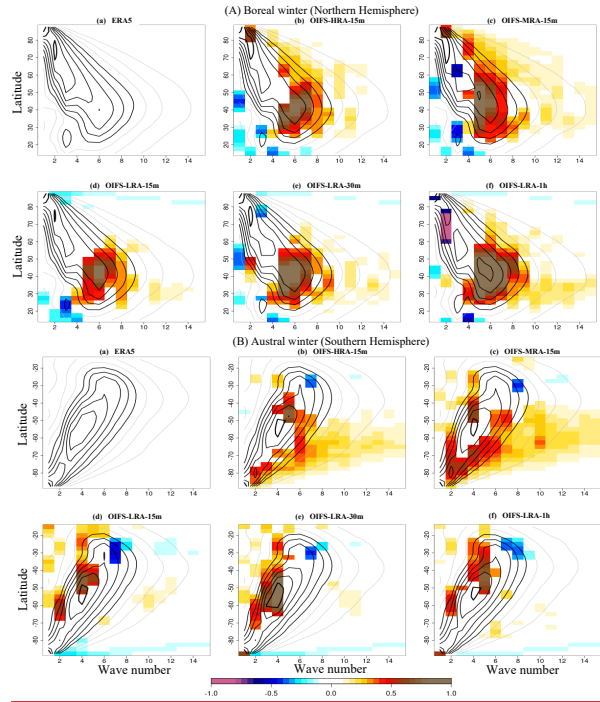
143 To verify our result, we computed the RMSE by smoothing the data and found a similar conclusion. However,
144 the RMSE values differ in magnitude if we compare them with without smoothing. We have not computed the
145 fraction skill score as our conclusions are insensitive to the double penalty effect (see the figure below; (left)
146 RMSE and (right) time mean Precipitation). We now added this information in the main text as well (lines 259-
147 263).

148 “We have computed the SAT and precipitation biases with a 3-point smoothing, i.e., approximately 3x3 degree
149 spatial smoothing, which eliminates the wiggles near steep topography arising from the Gibbs’ phenomenon in
150 the model spectral fields. We find that smoothing the fields does not change the main result that precipitation

151 biases increase with shorter time step in Tco95 and then decreases somewhat with higher horizontal resolution.
 152 Hence, the wiggles are not the main source of precipitation biases and their presence does not impact the
 153 findings in this study.”
 154
 155

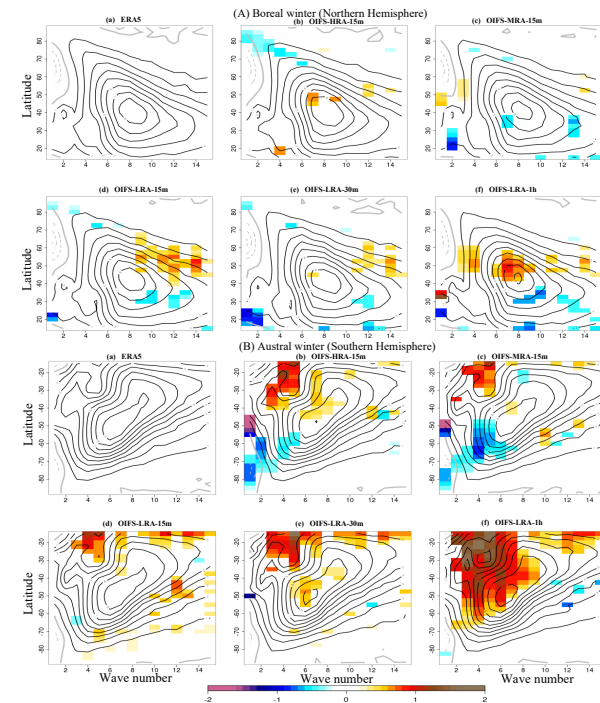


156
 157
 158
 159 Lines 237-238 and figure 4: Why do the authors standardise the wave amplitude biases in figure 4 instead of
 160 showing the absolute values? This standardisation emphasises errors in regions the authors argue are
 161 unimportant, which complicates interpretation of the plots. Specifically, the authors focus their analysis of
 162 Rossby waves on the "region where the wave amplitude is larger than 5 ms-1 is termed core region, which
 163 mostly covers the area that is occupied by the thick black contours in Fig. 4". However, biases are presented
 164 "relative to ERA5 (model – ERA5), normalized by the ERA5 detrended variability expressed by the standard
 165 deviation", which highlights errors in the high-latitude high-wavenumber waves that are dismissed by the
 166 authors as "unimportant as these waves have a small amplitude and little effect on variability".
 167 We updated the figures with absolute error and modified the texts accordingly (pages 9-10 and also provided
 168 texts below).
 169



170
171
172
173
174
175
176
177
178

Figure 5. (A) The Rossby wave amplitude (contours) for different wave numbers in the Northern Hemisphere at 300 hPa (a) in ERA5 observation and (b-f) in the OIFS model simulations during 1979-2019 in DJF (i.e., boreal winter). The color shows difference of wave amplitude between the model and ERA5 where it is significant on the 95 % confidence level. The wave amplitude and contour interval are shown in ms^{-1} . The grey contours start from 2 ms^{-1} and the black contours from 5 ms^{-1} and the contour interval is 1 ms^{-1} . (B) is similar to (A), but for JJA (i.e., austral winter).



179
180
181
182
183
184
185

Figure 6. (A) The Rossby wave phase speed (contours) for different wave numbers at 300 hPa in the Northern Hemisphere in ERA5 (a) observation and (b-f) in the OIFS model simulations during 1979-2019 in DJF (i.e., boreal winter). The color shows the difference of wave phase speed between model and ERA5 where it is significant on the 95 % confidence level. The wave phase speed and contour interval are shown in ms^{-1} . The black

186 contours start from 1 ms^{-1} and the contour interval is 1 ms^{-1} . Panel (B) is similar to panel (A), but for JJA (i.e.,
187 austral winter). The dashed contours show a negative phase speed and a grey contour shows a zero-phase speed.
188
189
190

191 “Fig. 5 shows the Rossby wave amplitude (gray and black contours) for ERA5 and the individual OIFS
192 simulations for the boreal winter (Fig. 5A, DJF, Northern Hemisphere; NH) and austral winter (Fig. 5B, JJA,
193 Southern Hemisphere; SH). The color in Fig. 5 denotes the wave amplitude bias relative to ERA5 (model –
194 ERA5). We focus only on those wave numbers and latitudes that have the highest wave amplitude, because these
195 waves explain most of the variability. The region where the wave amplitude is larger than 5 ms^{-1} is termed “core
196 region”, which mostly covers the area that is occupied by the thick black contours in Fig. 5. In DJF (NH), at north
197 of 70° N , the Rossby wave numbers $k=1$ and $k=2$ have the largest amplitude in ERA5 whereas at the mid-latitudes
198 (30° N to 60° N), the wave numbers between about $k=3$ and $k=9$ have large amplitude with the largest amplitude
199 amounting to 8 ms^{-1} at about 40° N for the wave number $k=6$ (Fig. 5Aa). During JJA (SH), the wave amplitude is
200 located in a similar core region (Fig. 5Ba) as that in DJF (NH). The amplitude is largest south of 70° S for the
201 wave numbers $k=1$ and $k=2$ whereas at the mid-latitudes (45° S to 65° S), the wave numbers between about $k=3$
202 to 5 have large amplitude with the largest amplitude amounting to 9 ms^{-1} is found at 57.5° S for the wave number
203 $k=4$ (Fig. 5Ba).
204

205 In DJF (NH) the OIFS-LRA-1h configuration exhibits a positive bias of $\sim 1 \text{ ms}^{-1}$ in Rossby wave amplitude (i.e.,
206 the waves amplitude bias in OIFS-LRA-1h is larger than the ERA-5) in the core region, in particular for wave
207 numbers $k=3-8$ at latitudes between 25° N to 55° N and a negative bias at latitudes between 60° N to 80° N for
208 waver number 2 (Fig. 5Af). The wave amplitude biases around the core region in OIFS-LRA-1h in the
209 midlatitudes (20° N to 40° N) are small (~ 0.2) for the higher wave numbers and get better with a shorter time step
210 configuration (OIFS-LRA-15m).
211

212 The Rossby wave amplitude biases in the OIFS-HRA-15m configuration are strongly reduced compared to the
213 OIFS-LRA-1h configuration over the core region (Fig. 5Ab and 5Af). The Rossby wave amplitude bias reduction
214 in the OIFS-MRA-15m configuration is mostly similar to that in the OIFS-HRA-15m configuration except for the
215 wave number $k=7$ at 45° N , where the wave amplitude bias is larger in the OIFS-HRA-15m configuration (Fig.
216 5Ab and 5Ac). The OIFS-HRA-15 m and OIFS-MRA-15m configurations also exhibit a positive bias for wave
217 number 2 at high-latitudes 60° N to 80° N . The OIFS-MRA-15m configuration also show a negative bias for the
218 wave number 3 at latitudes between 60° N to 65° N in the core region, which is not present in the other
219 configurations. The OIFS-HRA-15m and OIFS-MRA-15m configurations show similar bias around the core
220 region as in the OIFS-LRA-1h configuration, i.e., high resolution and OIFS-LRA-1h configurations overestimate
221 wave amplitudes for the higher wave numbers. The Rossby wave amplitude biases are progressively reduced from
222 the OIFS-LRA-1h configuration to the OIFS-LRA-30m and OIFS-LRA-15m configurations (Fig. 5Ad-Af),
223 indicating a sensitivity of model bias to the time step. The wave amplitude bias for wave number $k=7$ at 45° N
224 exists in all the configurations, and it is smaller in the OIFS-LRA-15m and OIFS-MRA-15m configuration than
225 in the other configurations. Overall, both OIFS-LRA-15m and OIFS-HRA-15m configurations are able to
226 reproduce the observed Rossby-wave amplitudes in DJF (NH) better than OIFS-LRA-1h.
227

228 In JJA (SH), the Rossby wave amplitude bias in the core region is smaller than in DJF (NH) for all the
229 configurations (Fig. 5A and 5B). OIFS-LRA-1h exhibits a positive bias of $\sim 0.5 \text{ ms}^{-1}$ in JJA (SH) for the wave
230 number $k=2$ at latitude between $\sim 50^\circ \text{ S}$ and $\sim 62.5^\circ \text{ S}$ and for wave numbers $k=4$ to 5 between 30° S and 40° S
231 (Fig. 5Bf). The OIFS-LRA-30m configuration shows a positive bias for the wave number $k=2$ to 5 at latitudes
232 between 40° S and 70° S , which is larger than other configurations.

233 The OIFS-HRA-15m and OIFS-MRA-15m configurations exhibits a positive bias $\sim 0.5 \text{ ms}^{-1}$ around the core
234 region and latitude 50° S to 70° S , which does not exist in the other coarse resolution configurations (Fig. 5Bb-
235 Bf). The Rossby wave amplitude biases around the core region at the midlatitudes in the high-resolution
236 simulations are consistent and large in the SH than the NH (Fig. 5Ab-c and 5Bb-c).
237

238 We also analyze the phase speed of Rossby waves for ERA5 and across the OIFS' configurations for DJF (NH)
239 and JJA (SH) seasons (Fig. 6). In the ERA5 dataset (Fig. 6Aa), the Rossby wave phase speed is positive (i.e.,
240 eastward moving, solid contour) for wave numbers greater than 2 (i.e., $k>2$) at most latitudes. The wave numbers
241 $k=1$ to 2 have a positive wave phase speed from the equator to 55° N and a negative wave phase speed (i.e.,
242 westward moving, dashed contours) between 60° N and 80° N in DJF (NH) (Fig. 6Aa). The maximum phase
243 speed is found at wave number $k=8$ at 40° N , while the minimum is found at wave number $k=1$ at 60° N (Fig.
244 6Aa). In JJA (SH) (Fig. 6Ba), the wave phase speeds are mostly positive and large for all the wave numbers and

245 at each latitude, with the maximum phase speed is observed for the wave numbers between $k=6$ and $k=8$ and
 246 latitudes between 40° S and 60° S, and these waves are moving faster than that in DJF (NH).
 247

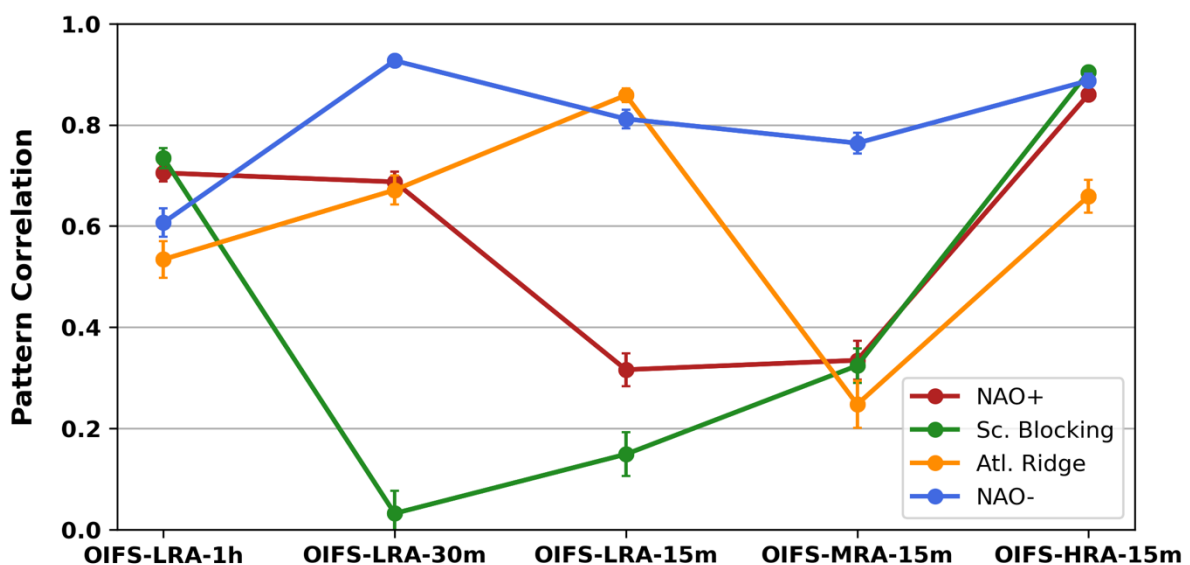
248 The OIFS-LRA-1h configuration suffers from positive phase speed bias for wave numbers $k=4$ to 8 at latitudes
 249 between 42.5° N and 60° N, i.e., waves move faster eastward than in ERA5, and the bias is larger than 1 ms^{-1} . The
 250 bias of $\sim 1 \text{ ms}^{-1}$ for wave number $k = 6$ to 8 at 40° N and 60° N is of particular concern as it is near the maximum
 251 wave amplitudes in DJF (Fig. 6Af). In general, phase speed biases in the OIFS-LRA-1h configuration are strongly
 252 reduced as either horizontal resolution is increased or time step is shortened (Fig. 6Ab-5Af). In JJA (SH), the
 253 OIFS-LRA-1h configuration exhibits a very large (between ~ 1.5 - 2 ms^{-1}) Rossby wave phase speed bias for most
 254 of the wave numbers, which is largest for the wave numbers $k=2$ to 8 between 15° S to 55° S (Fig. 6Bf). Large
 255 biases can be found between 15° S and 25° S ($\sim 1.5 \text{ ms}^{-1}$) for most of the wave numbers, but the wave activity is
 256 low there (Fig. 6Bf). The large phase speed biases are strongly reduced in the OIFS-LRA-30m and OIFS-LRA-
 257 15m configurations (Fig. 6Bd-Bf), indicating a strong sensitivity to the reduced biases in mean winds and wind
 258 speeds (Fig. 1). Overall, the Rossby wave speed bias in the OIFS-HRA-15m configuration is smaller than in the
 259 OIFS-LRA-1h configuration (Fig. 6Bb and 6Bf). However, we note that both the OIFS-MRA-15m and OIFS-
 260 HRA-15m configurations exhibit negative biases south of 55° S for wave numbers $k= 1$ to 5 , that is, the eastward
 261 moving waves are slower than in the ERA5 (Fig. 6Bb).
 262

263 The wave phase speed analysis reveals a clear improvement in the representation of the Rossby waves in the
 264 boreal winter (i.e., NH) when increasing the horizontal resolution and shortening the model time step compared
 265 to OIFS-LRA-1h configuration. In austral winter, however, the representation of Rossby wave amplitudes and
 266 phase speeds are the most realistic in OIFS-LRA-15m configuration, with longer time steps introducing too fast
 267 phase speeds and higher horizontal resolution introducing too slow phase speeds at wave number less than 6 (i.e.,
 268 $k < 6$).”
 269

270 Section 3.2. How do the authors interpret the impact on Rossby wave amplitude/phase speed biases? For
 271 example, is it related to the representation of tropospheric jets and associated wave guides and their biases?
 272 The representation of tropospheric jets and associated wave guides can be related to biases in Rossby wave
 273 packets (e.g., Giannakaki and Martius, (2016), Hakim, 2005 and Baumgart et al., 2018). We evaluate the
 274 amplitude and speed of each wavenumber individually that indicating at which scale the model biases occur.
 275 RWPs are then the combination (or sum) of the intermediate ones (e.g. wavenumbers 4-15), but
 276 diagnosing/tracking RWPs is a different analysis, and there's no consensus on the best method (Wolf and Wirth,
 277 2017).
 278

279 Section 3.3 and figure 7. What is the sampling uncertainty in these composites and estimates of pattern
 280 correlation (e.g. estimated using bootstrap resampling of available dates)? Are the differences between
 281 configurations significant?

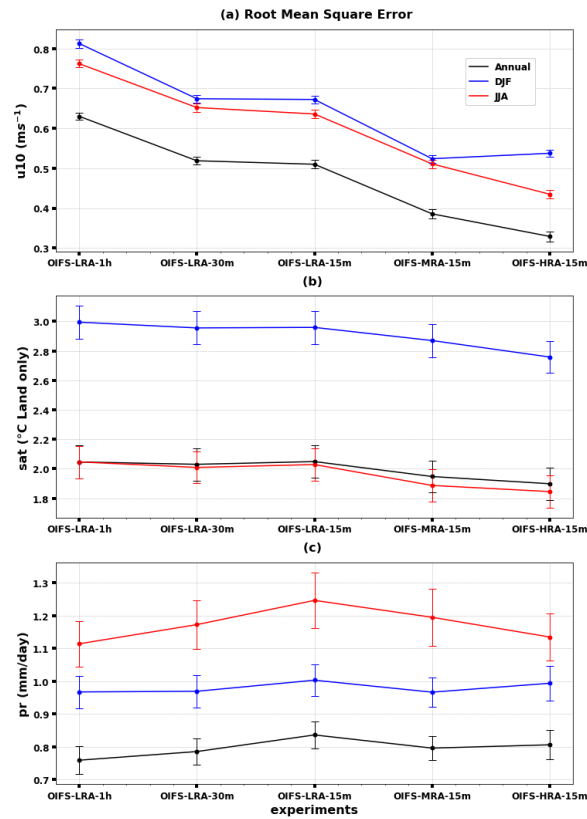
282 We added sampling uncertainty using bootstrapping method with random 2000 iterations.



283 Figure. 8. Pattern correlation coefficient of the individual weather regime between OIFS model configurations
 284 and ERA5 for the period 1979-2019 for the DJF season. The error bars represent a 95% confidence interval.
 285
 286

287 Table 1. What is the HPC cost of the different configurations (e.g. core hours per model year)? Do they scale as
 288 expected from changes in time-step and number of grid points?
 289 As the reviewer suggested, we added this information to Table 1 (lines 694-698).
 290

291 Figure 2. What is the sampling uncertainty in these estimates of RMSE? Are the differences in RMSE between
 292 configurations significant?
 293 We added the figure depicting RMSE with sampling uncertainty using bootstrapping method with random 2000
 294 iterations (see below and page 22).
 295



296 Figure 2. Root mean squared error of surface zonal wind (a), SAT (b), and precipitation (c) over the period 1979-
 297 2019 for all the configurations: annual (black) and seasonal mean (DJF: blue, JJA: red). The error bars represent
 298 a 95% confidence interval.
 299